Recombination models for spatio-temporal Monte Carlo transport of interacting carriers in semiconductors

Diksha Sharma,[1] Yuan Fang,[1,a)] Fahad Zafar,[1,b)] Karim S. Karim,[2] and Aldo Badano[1,c)]
[1]*Center for Devices and Radiological Health, Food and Drug Administration, 10903 New Hampshire Ave, Silver Spring, Maryland 20993 USA*
[2]*Department of Electrical and Computer Engineering, University of Waterloo, 200 University Avenue West, Waterloo, Ontario, Canada*

(Received 2 March 2011; accepted 19 May 2011; published online 16 June 2011)

When the secondary electron generated from an x-ray interaction within a photoconductor deposits energy, clouds of charge carriers (electron–hole pairs) with random spatial and energy distributions are created. Even under high electric field bias, a fraction of the carriers recombine affecting the detection statistics. We propose and compare modeling approaches for recombination including a nearest-neighbor model (NN) and a first-hit model (FH) that recombines the first pair from the vector of candidate carriers. We find that the mean of the NN model correlates with the mean of the FH model but differs for individual clouds. © *2011 American Institute of Physics*.
[doi:10.1063/1.3599602]

X-ray detectors based on semiconductor transducers are promising for emerging imaging technologies including breast tomosynthesis[1] and photon-counting mammography.[2,3] In addition, improved materials such as amorphous Se[4] and high-Z materials[5] are enabling energy discrimination approaches[6] in imaging. In recent work, we reported on a detailed transport code (based on previous work[7,8]) for the simulation of imaging devices.[9] However, one of the remaining fundamental aspects to be investigated in the modeling of x-ray photoconductor detectors is charge carrier recombination. In order to increase the detector sensitivity, a high electric field is typically used in amorphous Se devices to cause carriers to drift toward the electrodes, reducing recombination of electron–hole pairs (ehps) at the site of carrier generation and during transport. Increased recombination leads to fewer carriers contributing to the pixel signal, thus decreasing the detector quantum efficiency. In addition, variability in the recombination fraction (f, defined here as the ratio between the number of ehps recombined and the total number of ehps generated) is associated with increased detector noise, as reflected in a lower Swank (or information) factor[10] for energy-integrating detectors, and in broad energy-response functions[11] and event misclassification from spectral overlap, which degrades the spectral imaging performance, in energy-discriminating detectors.[12] However, a realistic model that incorporates recombination in the transport simulation has not been described in the literature. In this letter, we discuss different approaches to model the recombination processes in the framework of a spatio-temporal Monte Carlo transport code and apply these models to amorphous Se x-ray detection devices. We consider the physical accuracy of the algorithms as well as their computational efficiency, which is important for maintaining reasonable computing times for transport simulations.

When x rays interact with the semiconductor they deposit energy producing energetic secondary electrons through a variety of interaction mechanisms with energy dependent cross-sections. These energetic electrons lose their energy through a large number of low-energy-transfer events. In turn, the local deposition of energy produces a random spatial distribution of ehps called a *burst*. Each burst can have multiple realizations, called *clouds*, with a random distribution of initial ehp energies and positions. ehps lose their kinetic energy in a thermalization process and are initially separated by a finite distance, called the thermalization distance (d_0). This distance can be estimated for a given initial energy and applied electric field using the Knights–Davis equation.[13] For the purpose of this analysis, we consider a point burst, i.e., charge carriers initially lying on the surface of a sphere with an effective size (sphere diameter) given by d_0. This work is centered on the initial processes immediately after burst generation with regards to the transport and recombination of carriers. Later processes such as trapping and charge induction are not considered in this work.

Our spatio-temporal Monte Carlo code tracks individual carriers as they are transported in the material and checks for the presence of recombinations at finite time points separated by a constant time step Δt (for this work $\Delta t = 10^{-14}$ s). After the burst occurs, competing processes lead to the eventual collection at an electrode or recombination of these carriers.[14] Carriers are subjected to drift and diffusion. The drift component depends on the applied electric field ($\mathbf{E}$) and the Coulombic interaction between carriers. The effective electric field ($\mathbf{E}_e$) experienced by a carrier j is given by $\mathbf{E}_{e_j} = \mathbf{E} \pm \sum_{i=1, i\neq j}^{2N} \frac{q}{4\pi\varepsilon r_{ij}^2} \widehat{\mathbf{r}_{ij}}$, where N is the total number of ehps, q is the elementary charge (1.6022×10^{-19} C), ε is the dielectric constant of amorphous Se, r_{ij} is the distance between two carriers (cm) and $\widehat{\mathbf{r}_{ij}}$ is the unit vector representing the direction of the field from the charge carrier j and it depends on the charge carrier type. In addition, carriers experience Brownian motion with a diffusion length

[a)]Also at Department of Electrical and Computer Engineering, University of Waterloo.
[b)]Also at Department of Computer Science, University of Maryland Baltimore County.
[c)]Author to whom correspondence should be addressed. Electronic mail: aldo.badano@fda.hhs.gov.

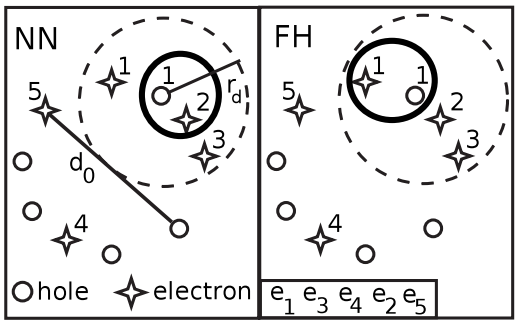

FIG. 1. Two-dimensional schematic of recombination models. The dashed line denotes recombination region for hole 1 (h_1). Electron table order is shown for the FH model. For NN, h_1 recombines with the nearest electron e_2 while for FH, it recombines with e_1, the first one in the table.

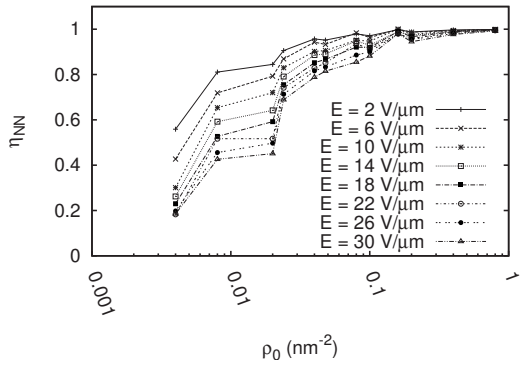

FIG. 2. Recombination efficiency of the NN model (η_{NN}) as a function of the burst carrier surface density $\rho_0=N/[4\pi(d_0/2)^2]$ under different bias conditions ($\mathbf{E}$=2 to 30 V/μm) for 1000 cloud realizations.

given by $L=\sqrt{6D\Delta t}$, where D is the diffusion constant (cm^2 s^{-1}) and Δt is the time step (s).[13] The total displacement is obtained by adding the displacements from drift and diffusion. Our transport models show excellent agreement for $N=1$ with results obtained using Onsager's theory.[15] A detailed description and validation of the physics models will be presented elsewhere.

Recombination events are determined at each time step using a recombination algorithm and, for simplicity, ignoring local variations in the field due to the material crystalline structure, i.e., the probability of recombination is modeled as proportional to the distance between recombining carriers. These recombination models are the focus of this letter. After recombination events are tallied, carrier transport resumes. The mean recombination fraction over many random clouds is denoted as the recombination efficiency (η).

We assume that recombination occurs if carriers are within a recombination distance (r_d) assumed in this work to be 1 nm. Our first model determines recombined pairs based on minimum distance between the carriers, considering one carrier at a time. We call this the *nearest-neighbor* model (NN). For a carrier, the distances are calculated for all possible candidates (oppositely charged carriers) and the nearest is marked for recombination leaving the rest of the candidates available for future recombinations. If we define the locations of all the electrons in the cloud as $\mathbf{e}=\{e_1,e_2,\ldots,e_N\}$, where N is the total number of ehps, then the subset of electrons lying within distance r_d from hole h_i is given by $\mathbf{e}^{h_i}=\{e_j \in \mathbf{e}: d(h_i,e_j)<r_d\}$, where $d(h_i,e_j)$ is the distance between h_i and e_j. Here, h_i will recombine with $e_{j'}^{h_i}$ such that $j'=\text{argmin}_j\, d(h_i,e_j^{h_i})$.

The NN model is implemented as follows: for a carrier h, all the recombining candidates are sorted using quicksort (intrinsic function) by their x coordinate. This allows for a rapid determination of all the recombining candidates within a 2-nm slab centered on carrier h. The recombining candidates within the slab are subsequently selected using their y and z coordinates to determine all candidates within a 2 nm cubic neighborhood of the carrier. The distance to all recombining candidates within the cube is calculated to determine the nearest neighbor for recombination, provided the minimum distance is less than r_d. This is repeated for every carrier. A schematic of the model is shown in Fig. 1. Using this model, we investigated the effect of the number of ehps (N), applied electric field ($\mathbf{E}$) and thermalization distance (d_0) on the recombination efficiency (η_{NN}) as a function of the surface density (ρ_0) of a cloud given by $N/[4\pi(d_0/2)^2]$ (see Fig. 2). The efficiency η_{NN} increases with larger ρ_0 due to greater availability of carriers for recombination and decreases with larger $\mathbf{E}$ which forces holes and electrons to separate toward the respective electrodes.

Because the NN model is computationally intensive, we developed an alternative model, the *first-hit* model (FH). The algorithm consists of looking at the recombining candidate table and selecting the first candidate at a distance less than r_d from the carrier. Once the algorithm finds such a recombining candidate, it identifies the pair as recombined and moves on to the next carrier in the list. Here, h_i will recombine with $e_{j'}^{h_i}$ such that j' is the lowest index (provided that $\mathbf{e}^{h_i}\neq\emptyset$). This is physically not as accurate as the NN model, because it finds a recombining candidate based on the table order which might not be the one nearest to the carrier (see Fig. 1).

Figure 3 depicts a comparison between the recombination fractions and efficiencies of the two models. We observe that for smaller d_0 and $\mathbf{E}$, where most of the carriers recombine, f_{NN} is very similar to f_{FH}, while for larger d_0 and $\mathbf{E}$, f_{NN} is uncorrelated with f_{FH}, even though their correspond-

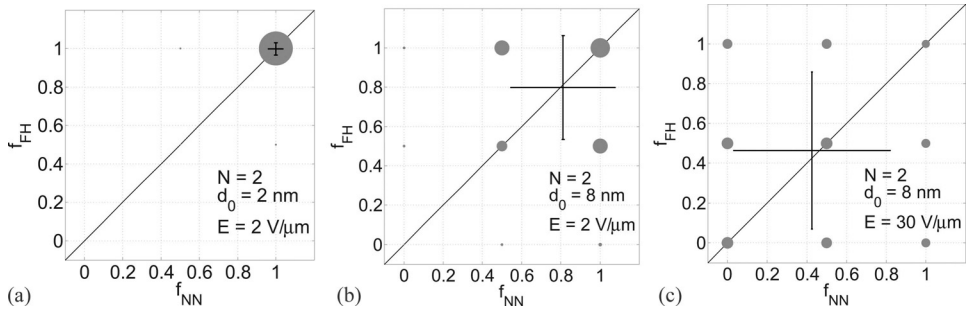

FIG. 3. Comparison of recombination results for 1000 cloud realizations. The size of the bubble represents the distribution of f_{FH} and f_{NN} for the 1000 clouds simulated. The recombination efficiency (η) for the two models are shown by the intersection of the black lines with the error bars depicting the standard deviation. For these figures, N=2 (a) d_0=2 nm, $\mathbf{E}$=2 V/μm, (b) d_0=8 nm, $\mathbf{E}$=2 V/μm, (c) d_0=8 nm, and $\mathbf{E}$=30 V/μm.

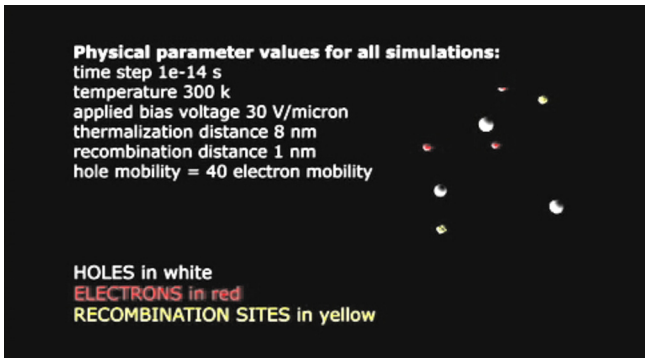

FIG. 4. (Color online) Still from video showing the physical parameters for the simulations rendered in the example cases. The visualization depicts the fate of two clouds, one for which the recombination factor does not change with the recombination model used to transport the ehps, and one for which the recombination factor significantly differs. (enhanced online). [URL: http://dx.doi.org/10.1063/1.3599602.1]

ing recombination efficiencies and standard deviations are similar.

To investigate the stability of the FH model with changes in the recombining candidate table order, we implemented a slight variation in the model which we refer to as FH *with shuffle*. In this model, the FH algorithm is repeated for a number of shuffles of the table corresponding to a given cloud. We observed that different shuffles result in different recombination fractions, as expected (see Fig. 4 for video).

We consider the NN model to be physically more realistic than the FH model while being more computationally demanding. The time taken for calculating only recombinations for 1000 random clouds with $N=10$, $d_0=8$ nm is 440 s for the NN model and only 35 s for FH, making NN 12.6 times slower than FH. For $N=10$, $d_0=2$ nm, NN is 30 times slower than FH (15 s vs 0.5 s). These timings correspond to a system based on single Intel®Core i7 920 Processor. Computational efficiency depends mostly on η and ρ_0. Our results suggest that NN is significantly slower than FH for the conditions tested. The ratio between the computing times for NN and FH might differ for simulations involving large η and/or large ρ_0. Running these simulations on multiple cores in parallel is complicated as the transport does not easily parallelize due to the intercarrier dynamic dependencies.

In addition, to investigate the stability of our models with respect to the time step (Δt), we calculated η for time steps of 10^{-12}, 10^{-13}, 10^{-14}, and 10^{-15} s. Preliminary results show that η is not affected for Δt values ranging from 10^{-13} to 10^{-15} s. A complete study of the temporal stability and its dependence on ρ_0, d_0, and N will be reported elsewhere.

To provide additional insight into these models, we have developed a visualization tool that allows for three-dimensional renderings of cloud histories from the generation of the carriers and their distribution in space, through the temporal evolution of positions and recombination events, until all pairs reach their fate (either recombined or detected at the electrodes). Sample cloud histories for the three models have been animated in a video (see Fig. 4).

In this work, we applied our models to the transport of carriers originating in a single, point burst generated by energy depositions from x-ray quanta interacting with amorphous Se devices. This approach can be extended to modeling multiple nonpoint (where all the carriers do not lie on the surface of a sphere but are rather randomly distributed in space) bursts corresponding to the same electron track, or the same primary incident x-ray. In this case, carriers from different bursts are allowed to interact with each other adding additional complexity and emphasizing the need to investigate computational efficiency gains that can be achieved by implementing a NN model in massively parallel Graphics Processing Units. In addition, the current model simulates transport and recombinations separately resulting in some redundant calculations which points to further optimization.

The authors are thankful to Andreu Badal and Christian Graff (CDRH/FDA) for their comments and suggestions. Y. Fang and F. Zafar were funded by the Research Participation Program administered by ORISE through an interagency agreement between DOE and FDA. This work was also supported in part (Y.F.) by the Carl A. Pollock postgraduate fellowship award. The mention of commercial products herein is not to be construed as either an actual or implied endorsement of such products by the Department of Health and Human Services.

[1]M. Bissonnette, M. Hansroul, E. Masson, and S. Savard, Proc. SPIE **5745**, 529 (2005).
[2]E. Fredenberg, M. Hemmendorff, B. Cederström, M. Åslund, and M. Danielsson, Med. Phys. **37**, 2017 (2010).
[3]H. Bornefalk and M. Danielsson, Phys. Med. Biol. **55**, 1999 (2010).
[4]S. Kasap and J. Rowlands, J. Mater. Sci. Mater. Electron. **11**, 179 (2000).
[5]S. Kasap and J. Rowlands, Proc. IEEE **90**, 591 (2002).
[6]N. Allec and K. Karim, Proc. SPIE **7622**, 76221M (2010).
[7]M. Lachaine and B. Fallone, J. Phys. D **33**, 1417 (2000).
[8]E. Fourkal, M. Lachaine, and B. Fallone, Phys. Rev. B **63**, 195204 (2001).
[9]Y. Fang, A. Badal, N. Allec, K. Karim, and A. Badano, Proc. SPIE **7622**, 762214 (2010).
[10]I. Blevis, D. Hunt, and J. Rowlands, Med. Phys. **25**, 638 (1998).
[11]A. Wang and N. Pelc, IEEE Trans. Med. Imaging **30**, 84 (2011).
[12]T. Schmidt, Med. Phys. **37**, 1056 (2010).
[13]J. Knights and E. Davis, J. Phys. Chem. Solids **35**, 543 (1974).
[14]W. Que and J. Rowlands, Phys. Rev. B **51**, 10500 (1995).
[15]L. Onsager, Phys. Rev. **54**, 554 (1938).